Revue Roumaine de Chimie, **2008**, *53*(2), 83–100

REVIEW

SYNTHESIS OF NANOSTRUCTURED MATERIALS BY MEANS OF THERMAL PLASMA. MODELLING OF THE PROCESSES

Emilia BALABANOVA

Institute of Electronics – Bulgarian Academy of Sciences,
Tzarigradsko chaussee 72, Sofia 1784, Bulgaria, emilia@iegate.ie.bas.bg

Received November 24, 2006

The thermal plasma is a partially ionized gas, that is characterized by high enthalpy i.e. very high temperature (thousands, K). This makes the thermal plasma a perfect agent for manufacturing any type of substances, but it is especially effective for high boiling temperature substances. The main processes, carried out in the thermal plasma setups, are vaporization and following vapor condensation. These processes lead to nanostructured materials formation. The specific characteristics (chemical and phase content, structure, size, etc.) depend on the conditions of the materials synthesis. It is very important for the synthesis that the processes are modelled and the optimum conditions for nanostructure formation found. In this lecture modelling the basic processes, taking place in the thermal plasma setups, is considered. Examples of ceramic nanomaterilas (Si-oxide, -nitride, -carbide and rare earth manganites) production are given.

INTRODUCTION

The thermal plasma is partially ionized but electrically neutral gas (as a whole). The gas ionization is obtained by the thermal heating, caused by electric discharges. Two types of discharges, electrodes (direct current (DC) electric arcs) or electrodeless (obtained by electromagnetic fields in Radio Frequency (RF) range) are used for thermal plasma formation. The electric power of the DC arc and of the RF discharges can be from some to hundreds kW, so the plasma has high enthalpy i.e. very high temperature (thousands, K). This makes the plasma a perfect agent for processing and synthesizing any type of substances, but it is especially effective for those characterized by a high boiling temperature. Recently, the specific conditions (thermal and gasdynamic), realized in the plasma setups, are considered as very suitable for nanostructured materials production. The fast vaporization of the raw substances and the following fast condensation are a very good way for production of materials in both forms – nanopowders or nanostructured coatings. It is important that the plasma devices allow manufacturing of large volumes of the substances (m^3) for a short time (seconds). This is the reason for using the thermal methods as preferrable for large industrial production of nanomaterials, especially of nanopowders.[1]

Before starting the industrial production, information about the processes, carried out in the plasma setups, has to be obtained. The important technological parameters and relations, e.g. process optimization parameters or relations between the initial process parameters and product characteristics, have to be studied. This can be done by carrying out a lot of experiments or by modelling. To make plasma experiments is a time and electric energy consuming task (the price of electricity is a still limiting factor). The modelling of the processes, taking place in the plasma setups, suggests a good opportunity to overcome the problem.

Different high temperature ceramic compounds such as oxides, nitrides, carbides etc. are obtained in nanostructured form by DC, or RF plasma methods. (Examples for such type productions can be found *e.g.* in the Proceedings of the world-known regular International Symposium on Plasma Chemistry, ISPC). The nanoproducts of these substances are advanced ceramic materials for automotive, aerospace, constructional etc. applications.

Recently, many efforts of the plasmachemists are aimed at synthesising special oxide materials *e.g.* such with a perovskite structure. Among these materials the rare earth (pure or doped) manganates are very interesting because of their specific electric and electronic properties. This materials are used as building element (cathode) of a new type electrical devices, so called Solid Oxide Fuel Cells (SOFC).[2]

In this paper the thermal plasma production of ceramic nanomaterials (Si-oxide, -carbide, -nitride), as well as rare earth manganites, is considered. The examples that are given are from our practice. The stress in the consideration is put on the modelling of the basic processes, taking place in thermal plasma setups.

Many years ago in the Institute of Electronics, BAS study of SiO_2 nanopowder production under the conditions of DC arc plasma was carried out, both experimentally and by modelling.

More recently, study of SiC and Si_3N_4, as well as pure or Sr doped La manganates production, by use of RF IC plasma was carried out in the Institute of Technical thermodynamics, DLR, Stuttgart, experimentally, and in the Institute of Electronics, BAS, by modelling. The Si-based non-oxide ceramics were produced in two forms – coatings and powders. The pure or Sr doped La manganates were produced as nanostructured coatings.

The modelling of the mentioned DC or RF plasma synthesis was already presented in our previous publications, so here only the main ideas and results will be given.

MODELLING THE PROCESSES OF SILICA NANOPARTICLE PRODUCTION BY DC ARC PLASMA

The silica powders, consisted of nanosized particles, have many different applications as fillers, lubricants, elastic gum reinforcing agents, catalytic basses etc. The successful application of the powders depends on the characteristics of the powders (*e.g.* particle size and structure). This information can be obtained by studying the processes, carried out in the plasma setups.

In Fig. 1 schema of the experimental setup for silica nanopowder production, used in our lab, is shown. The vaporization of the raw material (99.95% SiO_2) takes place in a stationer vaporizer by DC Ar arc plasma with electric power from 18 to 30 kW. After the vaporization, the silica vapour enters a flow reactor, where it is rapidly cooled by mixing it with a cooling gas, O_2 During the cooling the vapour condensation is taking place and nanoparticles are produced. Depending on the reactor conditions, powders with different (from 7 to 50 nm) nanoparticle mean sizes are obtained.

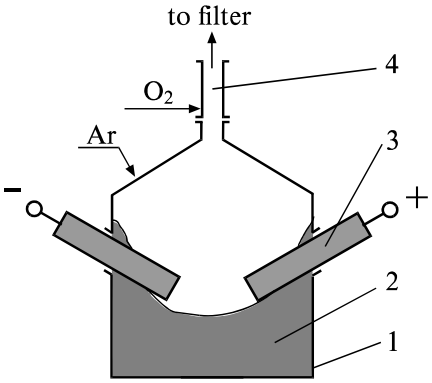

Fig. 1 – Experimental setup for silica nanoparticle production: 1 – plasma chamber, 2 – raw material (silica sand), 3 – electrodes (in some experiments – DC plasma generators), 4 – flow plasma reactor.

The processes, carried out in the vaporizer, as well as in the flow plasma reactor, were modelled and the results are discussed in detail in[3-9] Bellow the based model assumptions and some of the obtained more important results are presented.

1. Processes in the vaporizer. Thermodynamic modelling

In the vaporizer the silica sand is heated and converted to silica vapour. It is known that the silica vapour consists of SiO and O, *i.e.*, vaporisation is connected to chemical destruction, and consequently the effectivness of the vaporization process can be influenced by the use of reductors (*e.g.* C, H_2) which react with oxygen.

We consider the processes in the vaporizer to be carried out under the conditions of thermodynamic equilibrium and make some thermodynamic calculations, aiming to obtain the chemical equilibrium contents of the species in the vaporizer, as well as specific energy consumption for the vaporization of the raw substance.

Principally, the chemical contents of the species in a multi-component, multi-phase system can be obtained by numerical calculations, based on two different algorithms – "constant method" and "Gibss free energy minimization method". Description of both methods, applied to the plasma systems, can be found in.[10]

In "the constant method" the equilibrium content of the species in a chemically reacting

system, determined for defined temperature and pressure, is obtained by solving the set of equations for the equilibrium constants of all possible chemical processes in the system; equations of the elemental balance of the species in the system; equation of the mass conservation; ideal gas equation (normalization equation); equation of the charge conservation (if the system contains charge species).

In "the Gibss free energy minimization method" the chemical equilibrium is determined by minimization procedure of the Gibss free energy of the components in the system determined for the defined temperature and pressure. In this method there is no need to suggest the possible reactions. For the minimization are needed only polinoms, describing the Gibss free energy, and the information about the mole ratios of the initial components.

Our calculations for the chemical equilibrium contents of the species in the vaporizer were based on the constant method and we developed a special calculation program for the purpose.

We considered the following reactions as possible in the different cases of vaporization. Reactions (1-4) correspond to vaporization without reductors; reactions (1-7) – to vaporization with use of reductor H_2, and reactions (1-4, 8) – to use of reductor C.

$$SiO_{2(solid)} = SiO_{2(gas)} \quad (1)$$

$$SiO_2 = SiO + O \quad (2)$$

$$SiO = Si + O \quad (3)$$

$$O_2 = 2O \quad (4)$$

$$OH = O + H \quad (5)$$

$$H_2O = H + OH \quad (6)$$

$$H_2 = 2H \quad (7)$$

$$CO = C + O \quad (8)$$

The calculations of the chemical equilibrium contents of different chemical equilibrium systems were made in the temperature range 2000 – 4000 K for different mole ratios of the initial components: Ar (plasma gas); SiO_2 (raw substance); C, or H_2 (reductors).

The following initial mole ratios of the components were used: SiO_2 : Ar = 1:1, 1:2, 1:5; SiO_2 : Ar : H_2 = 1:1:1 and SiO_2 : Ar : C = 1:1:0.2, 0.5, 0.8, 1. The ratios were a priori chosen. The temperature was varied by step of 100 K. The pressure was taken equal to 1 atm, corresponding to the conditions in the experimental setup.

The calculated equilibrium contents for three different cases of SiO_2 vaporization are given as examples of the calculations in Figs. 2-4.

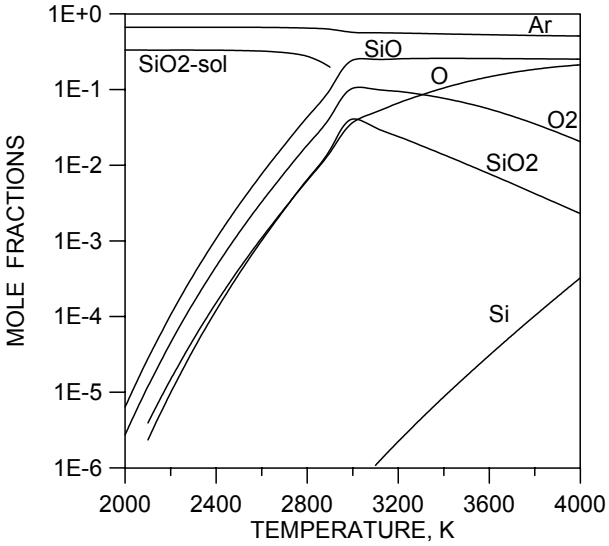

Fig. 2 – Equilibrium contents for the initial mole ratio SiO_2: Ar = 1: 2.

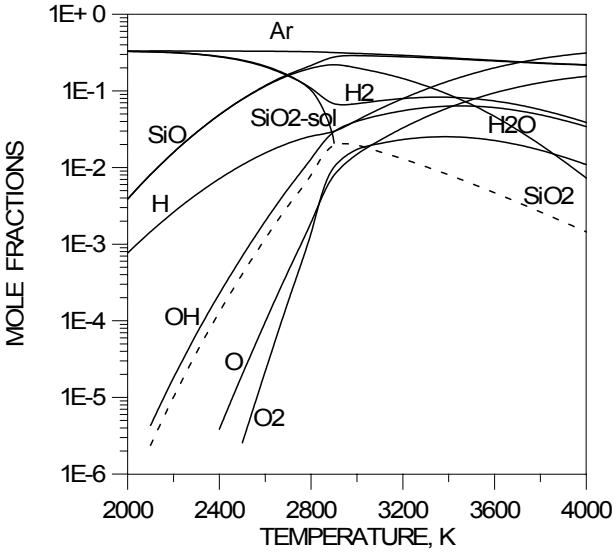

Fig. 3 – Equilibrium contents for the initial mole ratio SiO_2: Ar: H_2 =1:1:1.

As it was mentioned above, the thermodynamic consideration of the processes in the vaporizer allows the calculation of chemical equilibrium contents as well as, the calculation of the energy

consumption. The last is based on the following equations:

$$Q_g = Q / ag_i \tag{9}$$

$$Q = I_p - I_r \tag{10}$$

where: Q_g is the specific energy consumption of 1 kg raw material (kWh/kg), Q is the total energy consumption, kJ; g_i is the mass fraction of the raw substance, kg/mol; a is a coefficient to translation in kWh/kg.

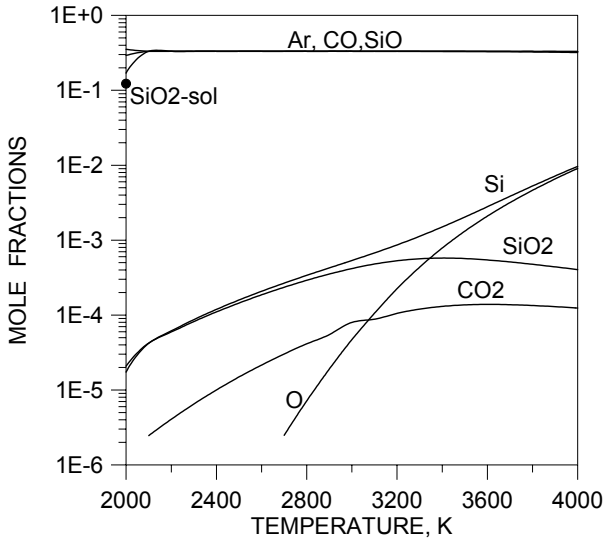

Fig. 4 – Equilibrium contents for the initial mole ratio SiO_2: Ar: C= 1:1:1.

$$I_r = \sum_{j=1}^{m} M_j I_j \tag{11}$$

$$I_p = \sum_{i=1}^{k} M_i I_i + \sum_{i'=1}^{l} M_{i'} I_{i'} \tag{12}$$

where: I_r is the total enthalpy of the raw species, kJ/mol; I_p is the total enthalpy of the products; I_j is the enthalpy of the j-th species; m is the number of the raw species; I_i, $I_{i'}$ are the enthalpies of the i-th and i'-th species; M_i , $M_{i'}$, M_j are the number of moles of i, i' and j species, respectively.

$$I_j = \Delta H_f(j,c,o) + \left[H^0(298.15) - H^0(0)\right] \tag{13}$$

$$I_i = \Delta H_f(i,g,o) + \left[H^0(T) - H^0(0)\right] \tag{14}$$

$$I_{i'} = \Delta H_f(i',c,o) + \left[H^0(T) - H^0(0)\right] \tag{15}$$

where: ΔH_f is the formation energy of the species (i, i', j) at 0 K; $H^0(0)$ the standard enthalpy, $H^0(T)$ and $H^0(298.15)$ are the enthalpies at given temperatures.

The thermodynamic calculations serve as a base for finding optimization parameters of the SiO_2 vaporization. These parameters are conversion degree of SiO_2 to SiO and specific energy consumption.

The conversion degree of SiO_2 to SiO (κ_{sio}, %) presentes SiO_2 destruction and it is considered as SiO_2 vaporization degree, too.

$$\kappa_{SiO} = \frac{x_{SiO}}{x_{SiO_2} + x_{SiO} + x_{Si}} 100\% \tag{16}$$

where: x_{SiO}, x_{SiO2}, x_{Si} are mole fractions of the corresponding species, obtained from the equilibrium contents calculations.

The other optimization parameter is presented as the energy need for vaporization of 1 kg of the raw material.

Both parameters, SiO_2 conversion (vaporization) degree (κ_{sio}) and specific energy consumption (Q_g), calculated for the different systems, are shown in Table 1. In the Table are given also the temperatures, at which the parameters are obtained. The shown temperatures are the temperatures of SiO_2 completely vaporization (*i.e.* there is no solid phase in the equilibrium mixture).

Table 1
Calculated optimum parameters of silica vaporization

initial ratios, moles	T, K	κ_{SiO}, %	Q_g, kWh/kg
SiO_2 : Ar = 1:1	3100	87.07	4.39
SiO_2 : Ar = 1:2	3000	88.93	4.38
SiO_2 : Ar = 1:5	3000	89.23	4.29
SiO_2 : Ar : H_2 = 1:1:1	3000	93.68	4.21
SiO_2 : Ar : C = 1:1:0.2	3100	89.22	4.39
SiO_2 : Ar : C = 1:1:0.5	3000	91.35	4.31
SiO_2 : Ar : C = 1:1:0.8	2900	96.73	4.23
SiO_2 : Ar : C = 1:1:1	2100	99.99	4.12

On the basis of the performed results (Table 1), the following can be concluded: the vaporization is influenced by the initial mole ratios of the components; the use of reductor C (in stoichiometric mole ratio to SiO_2) leads to a decrease of the SiO_2 vaporization temperature and also allows the vaporization to be carried out at high conversion rate and low energy consumption. (More about the role of the C in the silica nanoparticle production can be found in[9]).

2. Processes in the flow plasma reactor. Kinetic modelling

In Fig. 5, schematic presentation of the flow plasma reactor used for silica nanoparticle production is shown. In the reactor two flows are mixed, hot-containing plasma gas and silica vapour and cooling- (O_2, taken in big excess to the vapour).

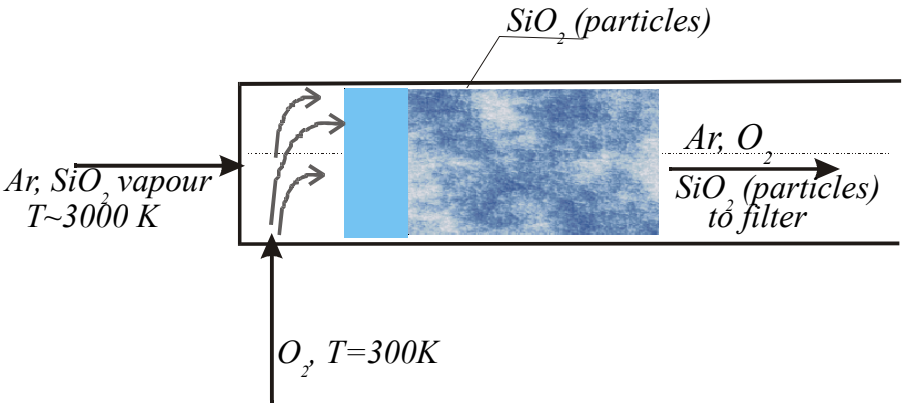

Fig. 5 – Schema of the flow plasma reactor for silica nanoparticle production.

Principally, the description of the phenomena, realized in the flow plasma reactor, is more complicated than that of the stationary vaporizer. Here, several processes (mixing, cooling, chemical reactions and condensation) are carried out simultaneously for a very short time (miliseconds). All processes, taking place in the reactor, are strongly time-dependant, so that the set of ordinary differential equations is used to describe them (the only argument is the time).

The developed model considers the generation of the nanoparticle precursor (monomer) by gas phase chemical reactions, as well as the monomer conversion to silica nanoparticles by condensation. The monomer formation and growth is realized under the non isothermal conditions during the mixing of two flows with extremely different temperatures. The description of the nanoparticle production by gas phase chemical reactions and homogeneous condensation at the constant temperature is described in the literature by the so called General Dynamic Equation. The adequate description of the condensation taking place simultaneously with the mixing and the cooling is still a problem. In our model we use several approximations, which are discussed bellow.

As a result from the model calculations the evolution of the particle size distribution function (PSDF) is obtained. PSDF presents the distribution of the number of particles, depending on their sizes. The PSDF is an important characteristics of the nanopowders, since its parameters (the mean particle diameter and the standard deviation) determine the nanopowder's dispersity. The influence of the different process parameters, such as initial monomer (SiO_2 gas molecule) concentration, cooling time *i.e.* time for the particle growth, etc. on the PSDF are investigated by the modelling.

For the further powder application it is important that the particle size and structure are known. For example, powders, having small sized non-aggregated particles, are good fillers in cosmetic and pharmaceutical products, while powders, containing large aggregates, can be applied as catalitic basis.

In[4-9] the modelling of the processes for silica nanopowder production in our plasma flow reactor is considered in details. The main model considerations and the more important results are presented bellow.

2.1. Modelling of the monomer (particle precursor) production

The following chemical reactions between silica vapour (SiO + O) and cooling gas (O_2), leading to production of SiO_2 gas molecules (the precursors of the nanoparticles) are taken into account:

$$SiO + O_2 \xrightarrow{k_1} SiO_2 + O \qquad (17)$$

$$SiO + O + O_2 \xrightarrow{k_2} SiO_2 + O_2 \qquad (18)$$

$$O + O + O_2 \xrightarrow{k_3} O_2 + O_2 \qquad (19)$$

The chemical reaction rates are presented by $w_1=k_1[SiO][O_2]$; $w_2=k_2[SiO][O][O_2]$ and $w_3= k_3[O]^2[O_2]$. Where k_1, k_2, k_3 are reactions rate coefficients.

The model equations representing the chemical processes are:

$$\frac{d[SiO]}{dt} = -w_1 - w_2 - \lambda [SiO] \qquad (20)$$

$$\frac{d[O]}{dt} = w_1 - w_2 - 2w_3 - \lambda [O] \qquad (21)$$

$$\frac{d[O_2]}{dt} = -w_1 + w_3 - \lambda [O_2] + g(t) \qquad (22)$$

$$S \equiv \frac{d[SiO_2]}{dt} = w_1 + w_2 - \lambda [SiO_2] \qquad (23)$$

where w_1, w_2, w_3 are chemical reaction rates, $g(t)$ is mixing function (its meaning will be discussed bellow), $\lambda=\alpha/T$ is a coefficient that takes into account the variation of the concentration with variation of the gas volume during cooling (the pressure in the reactor is constant, 1 atm); α is cooling rate, K/s; S presents the source of the monomers, (SiO_2 molecules).

2.2. Modelling the particle growth process

Considering the processes, responsible for silica nanoparticle production, special attention has to be paid to the processes of the particle growth. Most of the models, describing the nanoparticle growth from the vapour of the refractory raw substance, accept that the vapour is high supersaturated. In this case the particle growth is determined by the collision process between the species in the supersaturated vapour. The process is called free-molecular coagulation.

Since our model describes the formation of nanoparticles from refractory material (the boiling temperature of the silica is 3000 K) we also accept the free-molecular coagulation as the main process, responsible for the particle growth.

Different numerical methods are used for solving the free-molecular coagulation set of equations. Their advantages and disadvantages can be seen in.[1] We used discrete-sectional method[11] for describing the evolution of the particle size via free-molecular coagulation. The base assumption in the used numerical method is that particles are included in groups (sections) with masses m, 2m, 2^2m , 2^nm (m is the mass of the initial particle, monomer). The mass relates to the particle diameter because the particles are with spherical shape.

The set of free-molecular coagulation equations is given bellow. Equation (24) presents the evolution of concentrations of particles of group n and l. Equation (25) presents the evolution of the monomer concentration. Equation (26) gives the expression for coagulation coefficient, C_{nl}. In the equations z_n , z_l, z_0 , are the particle concentrations (cm^{-3}), M is the number of groups, ρ is mass density of the particles (2.2 g/cm^3 for silica particles), k is Botzmann's constant, T is absolute temperature.

$$\frac{dz_n}{dt} = \sum_{l<n-1} 2^{l-n} C_{l,n} z_n z_l + \tfrac{3}{4} C_{n-1,n-2} z_{n-1} z_{n-2} + \tfrac{1}{2} C_{n-1,n-1} z_{n-1}^2 - \sum_{l=n-1}^{M} C_{n,l} z_n z_l - \lambda z_n \qquad (24)$$

$$\frac{dz_0}{dt} = S - z_0 \sum_{l=1}^{M} C_{o,l} z_l - \lambda z_0 \qquad (25)$$

$$C_{n,l} = \left(2^{n/3} + 2^{l/3}\right)\frac{1+2^{n-l}}{2^n} F(m,\rho,T) \quad (26)$$

$$F(m,\rho,T) = 2^{1/6} 3^{2/3} m^{1/6} \pi^{1/6} \rho^{-4/6} (kT)^{1/2} \quad (27)$$

2.3. Modelling the mixing and the cooling processes

Two basic approaches are used for describing the mixing and the cooling processes.

In the first approach[4,5] a simple approximation of the mixing and cooling is accepted, namely instantaneous mixing (g(t) = 0) and constant cooling (α = -dT/dt = const).

Two cooling rates (α), 10^5 and 10^6 K/s, are accepted as typical for the considered reactor. The initial temperature of the hot flow is accepted to be 3000 K and the final temperature - 2000 K (it is SiO_2 solidification point). The initial monomer concentrations are considered to be $2x10^{17}$ and $6x10^{16}$ cm^{-3}. They relate to both typical ratios of the vapour and the cooling gas volumes, 1:10 and 1:25, respectively.

Based on the above initial data, and using the model equations, PSDF are calculated. It is obtained that PSDF are of a log-normal character, so the mean particle diameter is a mean median diameter. It is determined at PSDF=50%. Fig. 6 shows calculated PSDF for the both cooling rates and the both initial monomer concentrations. It can be concluded that if the processes are carried out with higher cooling rate and/or with lower initial monomer concentration, particles with smaller mean sizes can be obtained.

In the next approach,[6-9] the influence of the mixing on particle growth process is investigated. This approach is called "gradual mixing" because g(t) ≠ 0 and the cooling rate is not constant. In[6-7] an empirically found function (28) is used to present the variation of the cooling gas concentration, in the same time the temperature evolution is accepted a priori to be presented by the same function but with the opposite sign (29):

$$g(t) \equiv \frac{d[O_2]}{dt} = \frac{[O_2]_f - [O_2]_0}{2t_m} \sin\frac{\pi t}{t_m} \quad (28)$$

$$\alpha \equiv -\frac{dT}{dt} = \frac{T_E - T_o}{2t_c} \sin\frac{\pi t}{t_c} \quad (29)$$

where T_0 and T_E are the initial and final mean mass temperatures of the flow, respectively. $[O_2]_0$ is the initial O_2 concentration; $[O_2]_f$ is the final O_2 concentration reached at the mixing.

The type of functions (28, 29) are shown in Fig. 7a and 7b, respectively.

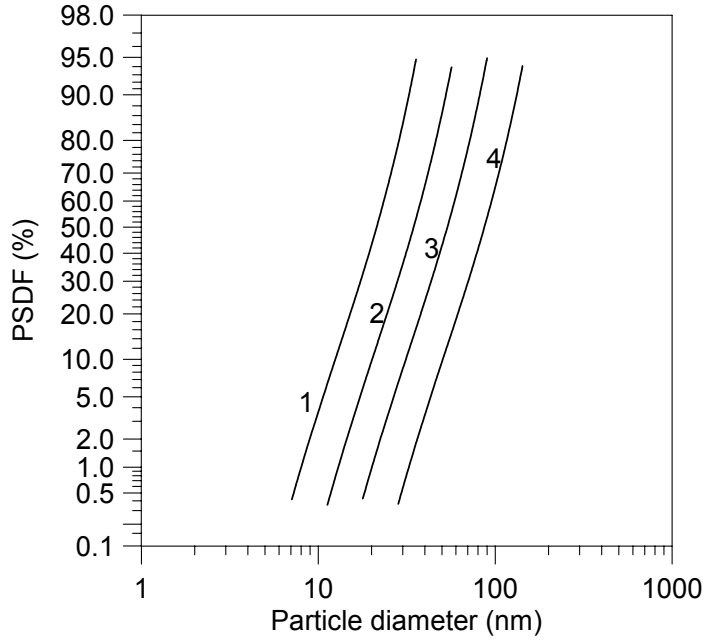

Fig. 6 – Integral PSDF calculated for initial monomer concentrations $6x10^{16}$ cm^{-3} and $2x10^{17}$ cm^{-3} at cooling rate of 10^6K/s (1, 2), at cooling rate of 10^5 K/s (3, 4), respectively. (The ratio silica vapour to cooling gas is 1:10 at the initial monomer concentrations $2x10^{17}$ cm^{-3} and 1:25 at -$6x10^{16}$ cm^{-3}).

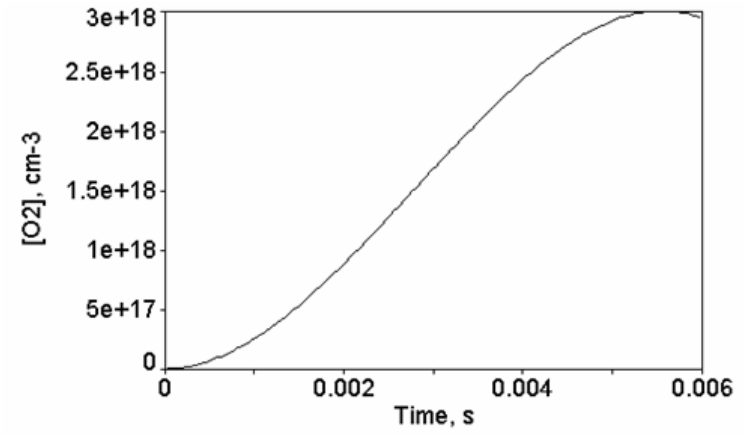

Fig. 7a – Variation of the cooling gas concentration.

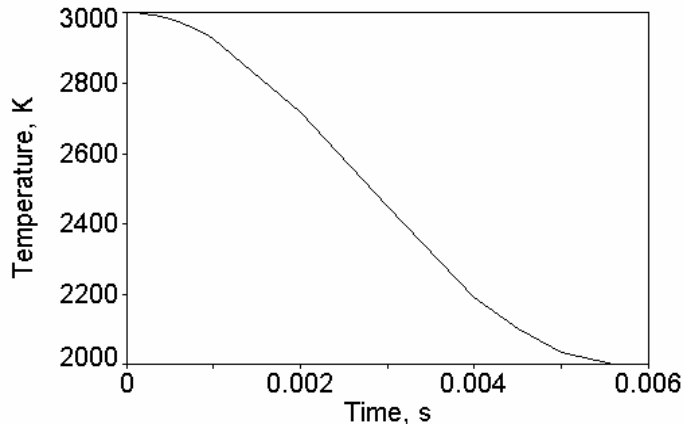

Fig. 7b – Variation of the mean mass temperature.

In Fig. 8 the calculated PSDFs in the case, considering the gradual mixing, are shown and are compared with those, obtained at the instantaneous mixing. It is known for the evolution of log normal PSDF that the self-preserving character is typical for the free-molecular coagulation mechanism of particle growth. As it is seen from Fig. 8, the mixing strongly affects the shape of PSDF i.e. particle growth process. A delay in the monomer generation and in the establishing of the self-preserving form of the PSDF is observed, due to mixing.

In both the above considerations (instantaneous mixing, gradual mixing), it was accepted a priory that the silica vapour is supersaturated at the beginning of the condensation process.

In the last approach[8-9] the influence of the mixing on the temperature and the vapour supersaturation is considered. The fluid dynamic equations, as well as mass and energy balances, are used for obtaining the flow velocity, the temperature and the species concentration variations (see equ. 30-35). Two types of mixing functions, linear (36) and non-linear (37) are used to present the mixing of the flows.

$$\frac{d(\rho u)}{dx} = \sum_{i=1}^{n} m_i g_i^{mix}(x); \tag{30}$$

$$\rho = \sum_{i=1}^{n} m_i c_i \tag{31}$$

$$\frac{dc_i}{dx} = \frac{g_i}{u} - \frac{c_i}{u}\frac{du}{dx} + \frac{g_i^{mix}(x)}{u};\ \text{i=1,.....n} \tag{32}$$

$$\frac{dp}{dx} + \frac{d(\rho u^2)}{dx} = 0; \tag{33}$$

$$p = RT\sum_{i=1}^{n} c_i \tag{34}$$

$$\frac{d}{dx}\left[u\left\{\frac{\rho u^2}{2} + \sum_{i=1}^{n} H_i(T)c_i\right\}\right] = \sum_{i=1}^{n}\left[g_i^{mix}(x)H_i(T^{mix})\right] \tag{35}$$

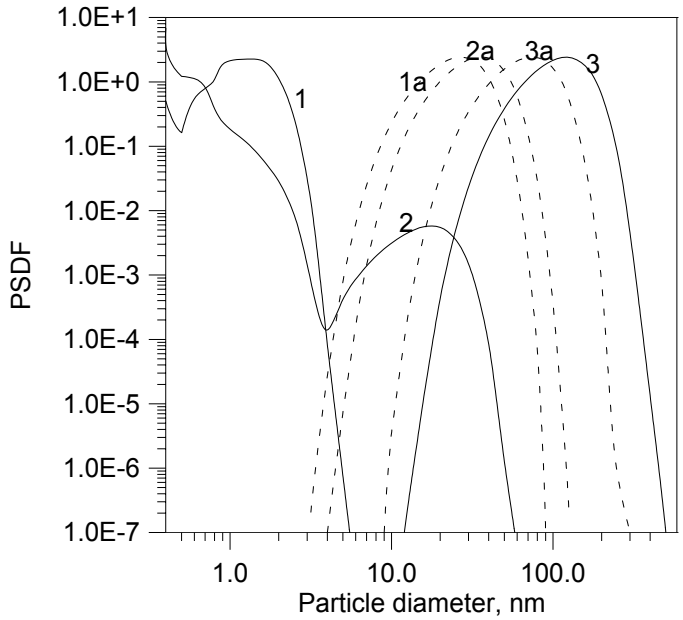

Fig. 8 – Evolution of the differential PSDFs calculated at times $0.5x10^{-3}$ s, $1x10^{-3}$ s and $5.6x10^{-3}$ s, during gradual mixing: 1, 2, 3; during instantaneous mixing 1a, 2a, 3a, respectively. (The ratio silica vapour to cooling gas is 1:10).

where x is the axial co-ordinate; u is the velocity; ρ is the density; T is the temperature of the gas mixture; T^{mix} is the temperature of the mixing gas; p is the pressure; R is the gas constant; n is the number of components; m_i, c_i, H_i, are the molecular mass, the volume concentration and the enthalpy of the i-th component, respectively; g_i, g_i^{mix} are the source terms presenting the variation of the i-th component quantity in unit volume in unit time due to chemical reactions and mixing, respectively.

$$g_{O_2}^{mix}(x) = \frac{g_2 - g_1}{x_2 - x_1} x \qquad (36)$$

$$g_{O_2}^{mix}(x) = \left\{ 1 - \cos\left[\frac{2\pi x}{x_2 - x_1} \right] \right\} \frac{g_2 - g_1}{x_2 - x_1} \qquad (37)$$

where x is axial co-ordinate; g_2 - g_1=1 is the full quantity of the mixing gas; x_2 - x_1 is equal to the mixing length.

In the frame of this "fluid dynamic approach" [8] the role of the type of mixing (linear, non-linear) on the particle growth is studied. It is obtained that: i) the mixing influences the temperature evolution in the flow reactor, which on its turn influences the variation of the monomer (SiO_2-gas molecule) concentration; ii) the time for the SiO conversion (oxidation) depends on the type of O_2 mixing too. At the linear mixing, the oxidizing time is shorter than that at the non-linear mixing. After the complete SiO oxidation, the vapour saturation is observed. The supersaturation is not reached immediately but its value varies with variation of the temperature in the reactor.

PSDFs are calculated for three different vapour saturations (7.6, 75, 195) reached at three temperatures of the flow: 3000 K, 2710 K and 2590 K, respectivelly, in the case of linear and non-linear mixing. The calculated PSDFs are shown in Fig. 9. It is seen that the mean particle diameter, determined at PSDF=50%, is smaller in the cases of higher supersaturations, as well as in the case of linear mixing. The same Figure also shows the experimental PSDF of the sample, produced at the same initial conditions. A reasonable agreement between the calculated and the experimental mean size is obtained, especially in the cases of fastest cooling and highest supersaturation.

In the frame of the fluid dynamic approach, except for the role of the mixing, the special role of the carbon in the nanoparticle formation and growth is considered in.[9] It is obtained that the use of C as reductor for silica sand vaporization strongly affects not only the vaporization process (decreasing its temperature) but also the particle formation process, leading to the production of aggregated silica nanoparticles (this model prediction is found out to be confirmed from the experiments).

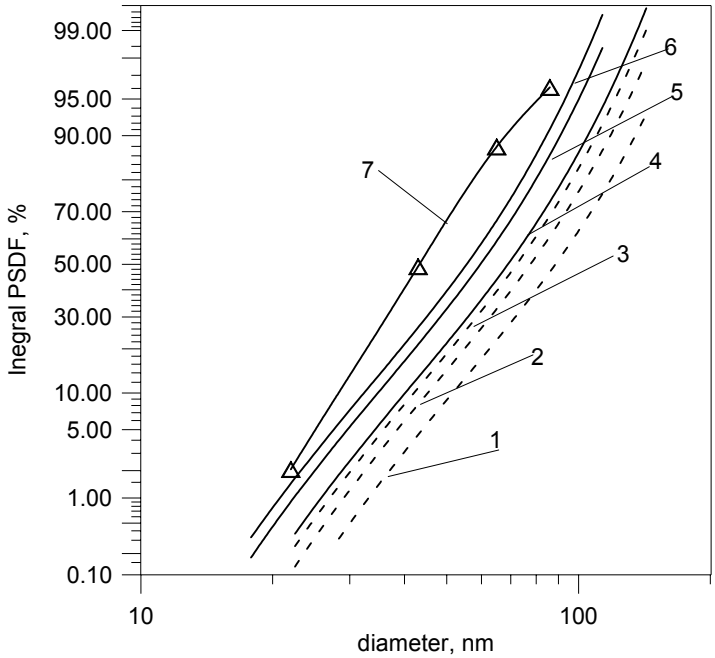

Fig. 9 – Final integral PSDFs calculated by fluid dynamic model, for linear mixing (1, 2, 3) for non-linear mixing (4, 5, 6); experimental PSDF (7). (The ratio silica vapour to cooling gas is 1:10).

3. Conclusions from the modelling of the processes of silica nanoparticle production

The modelling of the processes in thermal DC arc plasma setup is important because: i) it helps the better understanding of the condition**,** realized in the setup**,** and their influence on the particle growth mechanism; ii) by the modelling optimization parameters for the raw substance vaporization**,** as well as relations between the process parameters of the flow reactor and particle characteristics, can be obtained.

MODELLING OF THE PROCESSES OF Si-BASED CERAMICS PRODUCTION UNDER THE CONDITIONS OF RF PLASMA

The production of Si based ceramics (SiC, Si_3N_4) is interesting because of their well wear-, corrosion-, and high temperature resistance. The Si-based ceramics are advanced ceramic materials that can be synthesized under thermal plasma conditions in both forms: as nanostructured powders and as coatings. One very effective thermal plasma method for nanostructured coating production by use of liquid precursors is suggested by E. Pfender and co-workers.[12] This method, called thermal plasma chemical vapour deposition (TPCVD), gives the opportunity for a fast vaporization, followed by chemical reactions, and condensed phase deposition on the substrate.

In DLR Stuttgart, Germany, experiments for Si-based ceramics production by TPCVD were made in Radio Frequency Inductively Coupled Plasma (RF-ICP) setup. The maximum power of the RF discharge generator is 60 kW. The precursors are different types of chlorosilanes. The produced nanostructures have grain sizes between 20-40 nm for SiC and around 80 nm for Si_3N_4. The experiments are described in.[13-14]

The processes, carried out in the plasma setup, and leading to SiC and/or Si_3N_4 synthesis are complex. Their understanding starts with thermodynamic modeling.[15] The thermodynamic calculations were made for the precursor, CH_3SiCl_3 (volume flow rate 0.8 – 3 ml/min). The plasma gas was a mixture of either Ar/H_2 or Ar/N_2, taken in different ratios. The Ar is precursor atomization gas and its volume flow rate is taken to be 3 slpm.

1. Thermodynamic calculations

The chemical equilibrium in the systems Si-C-H-Cl-Ar and Si-C-H-Cl-Ar-N is considered with the aim to investigate the conditions under which the SiC and Si_3N_4 solid phases can be obtained.

A variant of the commercial thermodynamic program "ASTRA"[16] is used for the calculations of the chemical equilibrium contents in the considered systems. The program is based on Gibss free energy minimization algorithm and calculates the thermodynamic equilibrium in the systems, containing large number of components.

1.1. Calculations for the system Si-C-H-Cl-Ar

The chemical equilibrium compositions are calculated for 25 different cases of the system Si-C-H-Cl-Ar. They are determined for initial moles of the Ar = 3.48, the H_2= 0.22 and for 5 different initial moles of the row substance, CH_3SiCl_3, (0.007, 0.015, 0.017, 0.021, 0.026). Five different values of the pressure are taken (10, 20, 30, 40, 50 kPa). The temperature is varied in the range 500-3000 K by steps of 100 K.

The calculations are presented in[15]. They show that the equilibrium mixtures for all the considered 25 cases contain up to 40 to 42 species, among which are observed two solid species SiC and C. Example the equilibrium contents, at pressure of 10 kPa and CH_3SiCl_3 initial concentration of 0.017 mole, is shown in Fig. 10.

Examples of the influence of the different pressures (Fig. 11) and the different CH_3SiCl_3 initial concentrations (Fig. 12), on the variation of solid species concentrations can be seen.

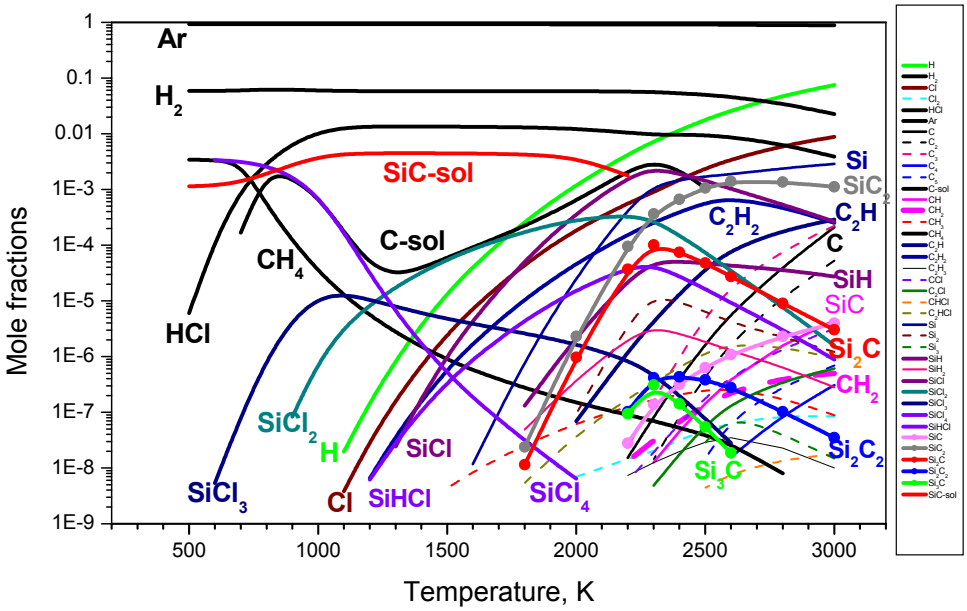

Fig. 10 – Chemical equilibrium composition calculated for the initial conditions of the case 313 (pressure 10kPa, CH_3SiCl_3=0.017 mole).

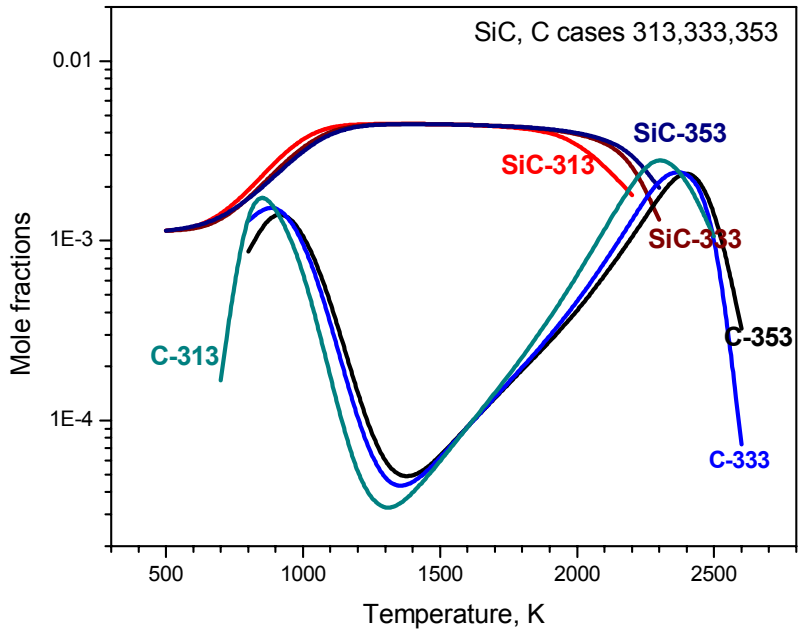

Fig. 11 – Variation of the solid species (SiC and C) concentrations for the cases: 313 (pressure 10kPa, CH_3SiCl_3=0.017 mole); 333 (pressure 30kPa, CH_3SiCl_3 =0.017 mole), 353 (pressure 50kPa, CH_3SiCl_3=0.017 mole).

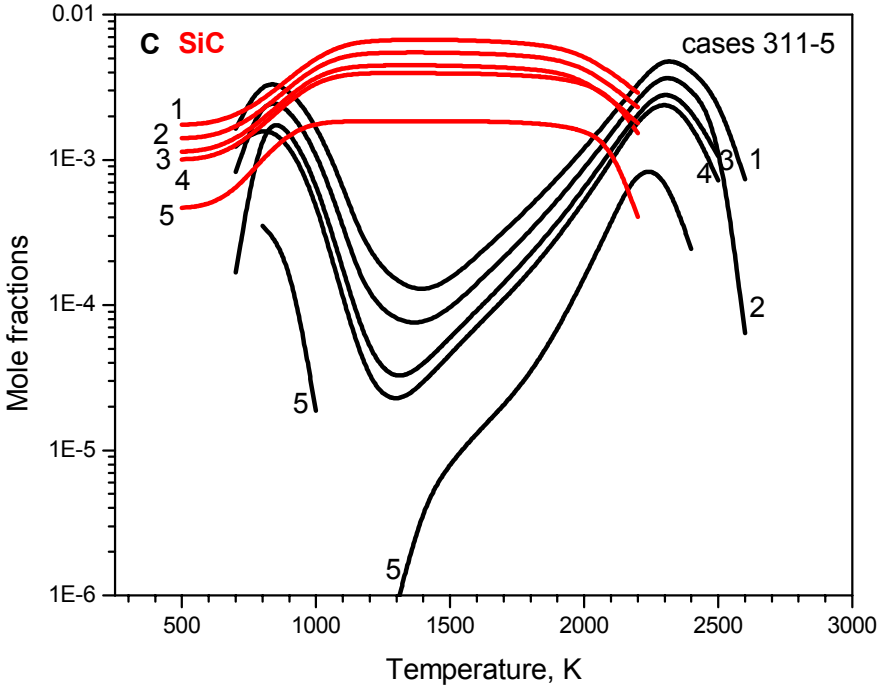

Fig. 12 – Variation of the solid species (SiC and C) concentrations at pressure 10 kPa for initial CH_3SiCl_3 concentrations: 0.026 mole (lines 1); 0.021 mole (lines 2); 0.017 mole (lines 3); 0.015 mole (lines 4); 0.007 mole (lines 5).

The obtained results allow the following conclusions to be made. In all considered cases, the equilibrium mixtures contain both SiC and C in a wide temperature range The variation of the pressure does not influence the production of the solid species (Fig. 11). The variation of the initial CH_3SiCl_3 concentration leads to the following: around 1300-1400 K, C-solid has a minimum, which is very deep in the case of the lowest CH_3SiCl_3 concentration (curve 5, Fig. 12), in the same time the SiC concentration has reached a plateau. At higher (2200-2300 K) as well as at lower (800-900 K) temperatures it is possible to fix equimolar mixtures of SiC and C. Below 800 K only SiC can be fixed.

1.2. Calculations for the system Si-C-H-Cl-Ar N

In the system Si-C-H-Cl-Ar-N the possibility for Si_3N_4, synthesis by use of N_2 is studied.

The N_2 is taken as addition to the plasma gas Ar (other investigators usually applied NH_3 , not N_2 as regent in Si_3N_4 plasma synthesis). The atomizing gas of the precursor CH_3SiCl_3, is Ar.

As in the previous system, equilibrium compositions of 25 cases are calculated, depending of the different initial conditions, namely: 5 different pressures and 5 initial CH_3SiCl_3 concentrations (the pressures and the concentrations are the same as in the previous system); Ar = moles, and N_2 = moles. The results from thermodynamic calculations[15] show that in all cases, three solid species (SiC, C and Si_3N_4) are observed in the equilibrium mixtures. The total number of the species for each of the equilibrium composition reached 52. An example of calculated composition i.e. this one, obtained at pressure of 10 kPa, and CH_3SiCl_3 initial concentration of 0.017 mole, is shown in Fig. 13. It is seen that Si_3N_4 is formed at temperatures lower than 1300-1400 K, near these temperatures both SiC and Si_3N_4 can be fixed.

The influence of the initial parameters on the solid species and especially on the desired product (Si_3N_4) formation, is studied. It is obtained (see Figs. 14 and 15) that the pressure, as well as the initial CH_3SiCl_3 concentration, influence the solid species production in the same way as it was observed for the system Si-C-H-Cl-Ar. A comparison between the temperature range, in which SiC is fixed in the system Si-C-H-Cl-Ar, and in the system Si-C-H-Cl-Ar-N leads to the conclusion that SiC is fixed in higher temperature range (1400-2400 K) in system when N_2 is used as plasma gas. The experimental results also show that the use of N_2 favors the formation of the SiC high temperature phase (α-SiC).[14]

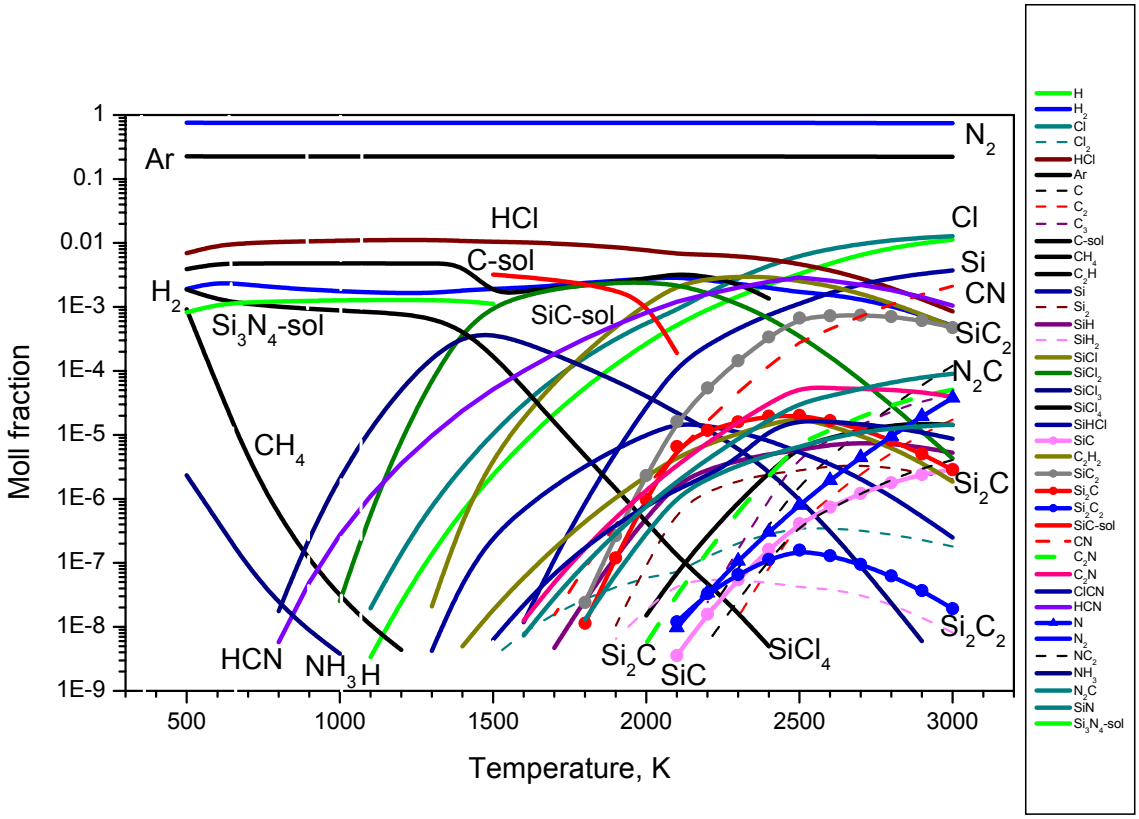

Fig. 13 – Chemical equilibrium contents calculated for the case N60- 313 (pressure 10 kPa, CH_3SiCl_3=0.017 mole).

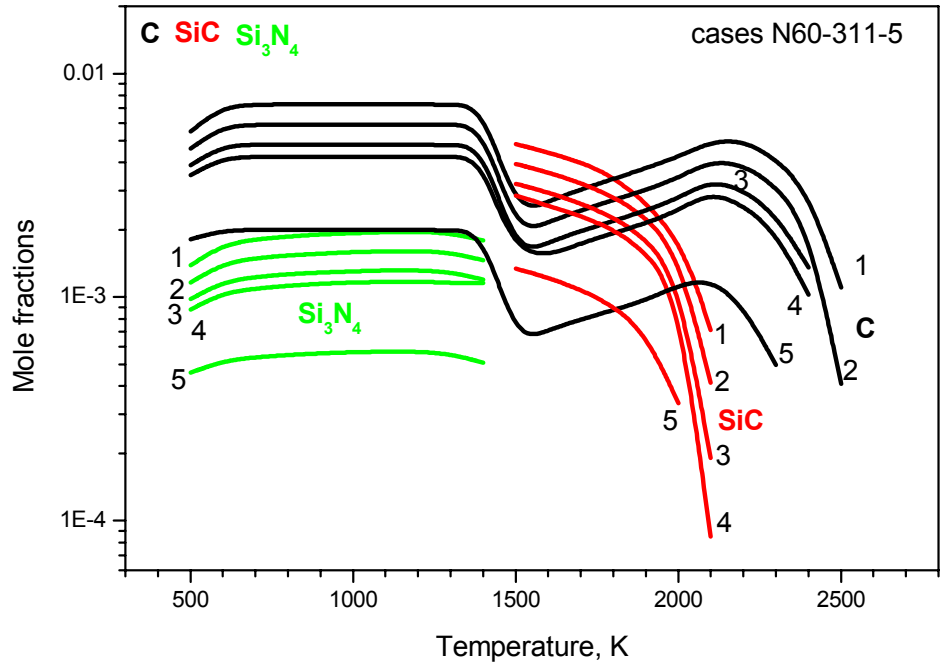

Fig. 14 – Variation of the solid species (SiC, Si_3N_4 and C) concentrations at pressure 10 kPa for the initial CH_3SiCl_3 concentrations: 0.026 mole (lines 1); 0.021 mole (lines 2); 0.017 mole (lines 3); 0.015 mole (lines 4); 0.007 mole (lines 5).

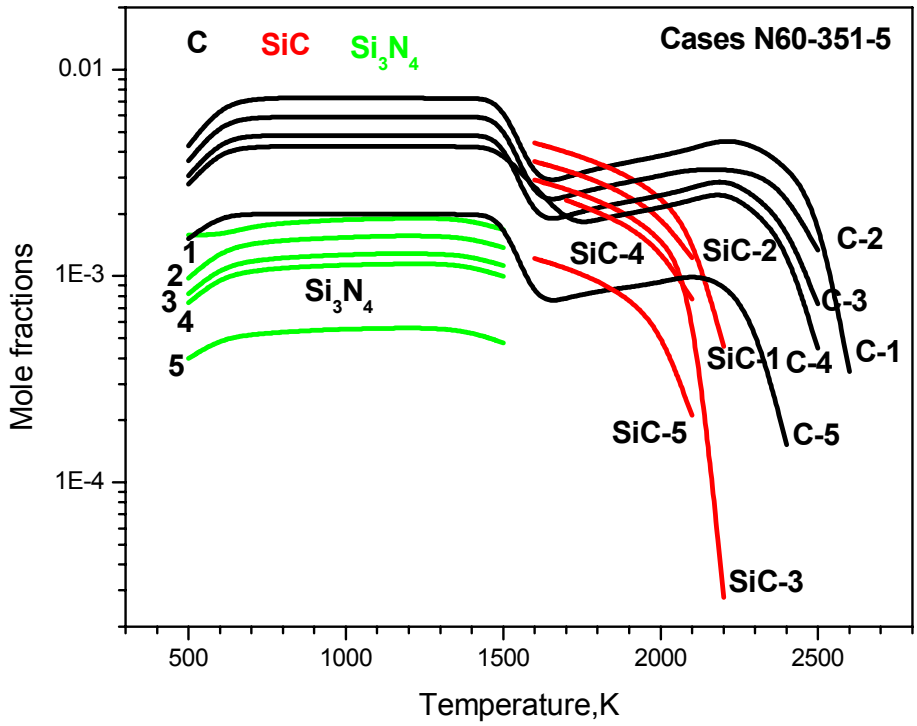

Fig. 15 – Variation of the solid species (SiC, Si_3N_4 and C) concentrations at pressure 50 kPa for initial CH_3SiCl_3 concentrations: 0.026 mole (lines 1); 0.021 mole (lines 2); 0.017 mole (lines 3); 0.015 mole (lines 4); 0.007 mole (lines 5).

2. Conclusions from the modelling of the processes of si-based ceramics production

The performed thermodynamic calculations show the conditions (temperature intervals, pressures, initial raw substance concentrations) under which SiC and Si_3N_4 can be produced in thermal RF IC plasma setups. The influence of the plasma reactor parameters on the chemical and phase contents of the produced species is obtained from the calculations. These calculations serve for obtaining preliminary information about the possibility of SiC and Si_3N_4 substances formation from liquid silane precursor under thermal plasma conditions. The mechanism of SiC, as well as Si_3N_4 coatings formation in TPCVD method**,** needs kinetic and hydrodynamic modelling**,** in which corresponding factors should be taken into account.

MODELLING OF THE PROCESSES OF La, (La, Sr) MANGANITE PRODUCTION UNDER THE CONDITIONS OF RF PLASMA

Ceramic materials with perovskite type structure, based on the La manganite, are interesting for investigation due to their wide range of elemental and stoichiometric composition, resulting in specific electronic, electric and magnetic properties of these materials.[17-19] Doped lanthanum manganite is recognized as a perfect cathode material for SOFC.

Recently, one-stage plasma methods**,** using liquid precursors (solutions) are applied to rare earth manganites coating synthesis.[20-22] TPCVD is considered to be much promising because it allows a fine tuning of the initial solution concentrations, leading to production of coatings with controlled elemental content, stoichiometry, as well as nanostructure. By this method the cathode of SOFC can be synthesized in one stage with controlled elemental composition and porosity. Thermodynamic investigations help for better understanding of the possibility of the perovskite formation.

1. Thermodynamic calculations

In our publications[23,24] a thermodynamic estimation of the possibility for La, and (La, Sr) manganites formation under thermal plasma conditions is made. In[23] the production of $LaMnO_3$

is disscused, but in[24] the possibilty for doped manganites (stoichiometric – $La_{1-x}Sr_xMnO_3$, and substoichiometric $La_{0.65}Sr_{0.3}MnO_3$) is considered. The calculations are related to the TPCVD experiments, carried out at DLR Stuttgart, Germany. The experimental setup is the same as the one, used for Si-based ceramics production. More about the experiments can be found in[21]. The operating pressure in the system is 20 kPa. The precursors, used for $LaMnO_3$ synthesis are aqueous solutions of $La(NO_3)_3$• $6H_2O$ and $Mn(NO_3)_2$• $4H_2O$ with concentrations of 1 M. The precursors, used for $La_{1-x}Sr_xMnO_3$ formation are aqueous solutions of: $La(NO_3)_3$•$6H_2O$ with molar concentration (1-x) M; $Sr(NO_3)_2$ with molar concentration x M; $Mn(NO_3)_2$•$4H_2O$ with molar concentration 1 M, where x takes the values of 0.1, 0.2. The precursors for $La_{0.65}Sr_{0.3}MnO_3$ formation are aqueous solutions of: $La(NO_3)_3$•$6H_2O$ with molar concentration 0.65 M; $Sr(NO_3)_2$ with molar concentration 0.3 M; $Mn(NO_3)_2$•$4H_2O$ with molar concentration 1 M. The precursor atomizing gas is Ar. The plasma gas in the all experiments is Ar, to which H_2 or O_2 is added in various ratios. The aim is manganites formation under reducing and oxidizing atmosphere to be studied, respectively.

The thermodynamic calculations are made by use of a variant of the thermodynamic program "ASTRA".[16] The equilibrium contents of system (LMO): La, Mn, H, O, Ar and LSM system, ULSM (La, Sr, Mn, H, O, Ar) under different initial conditions are obtained.

As most of the standard commercial thermodynamic programs, the used program calculates the equilibrium contents of the mixtures, consisting of individual species (gaseous, solids), but it does not calculate the contents of the solid solutions. It is known from the phase diagram[25] that $LaMnO_3$ is not a stable (line) compound, but it is accepted to be a solid solution of La_2O_3 and Mn_2O_3 (Mn_3O_4). The possibility for $LaMnO_3$ formation, *i.e.* the solid solution region, is determined by the ratio Mn/(Mn+La) and by the temperature.

For the Sr doped La-manganites temperature dependent phase diagram can not be found in the literature. The doped structures are considered as formed in the systems, containing La_2O_3, Mn_2O_3 (Mn_3O_4) and SrO.[26] In these systems the estimation of the possibility for Sr doped La manganite formation can be made by calculation of the ratios Mn/(La+Mn) and La/(La+Sr) as it is done in[26] and,[27] respectively.

Some of our results, concerning the possibility for pure and doped La manganites formation under thermal plasma conditions, are shown bellow.

1.1. Calculations for the LMO system

The equilibrium contents for the LMO system are calculated for three different initial conditions (cases: LMO-1, LMO-2, LMO-3).[23] The temperature is varied in a wide range 3000 - 300 K by decreasing in steps of 100 K.

The LMO-1 case corresponds to the experiment for manganite synthesis carried out in a reducing atmosphere (H_2 is used as addition to the plasma gas). In the LMO-2 and LMO-3 cases, the possibility for manganite formation in oxidizing atmosphere is considered. Two different O_2 amounts are used as additions to the plasma gas.

The results show that in the LMO-1 case it is difficult to predict $LaMnO_3$ formation, since under the reducing conditions, the Mn can not reach the high oxidation state (Mn^{3+}), typical for the La-Mn perovskite structures. In the equilibrium mixture, Mn is in the form of Mn^{2+}. The observed Mn – oxide in the equilibrium mixture is MnO, only.

In the cases (LMO-2, LMO-3) the observed solid oxides in the equilibrium mixtures are La_2O_3(s), MnO(s), Mn_3O_4(s), MnO_2(s). The important for perovskite structure formation are La_2O_3(s) and Mn_3O_4(s), *i.e.* the ratio Mn/(La+Mn). The calculation of this ratio and its comparison with the data from the phase diagram[25] leads to the next conclusions (see Fig. 16): i) La manganite perovskite can be fixed in a wide temperature range 1500 –900 K, or 1300 –800 K, depending on the amount of oxygen added to the plasma gas; ii) the occurrence of undesired La_2O_3 is hard to be overcome in these temperature ranges (this result is experimentally observed also;[22] iii) the use of 10 times excess of O_2 (case LMO-3) favors the synthesis of pure $LaMnO_3$ (without contamination of La_2O_3) at relatively high temperature of 1600 K (this result is important for planning future experiments).

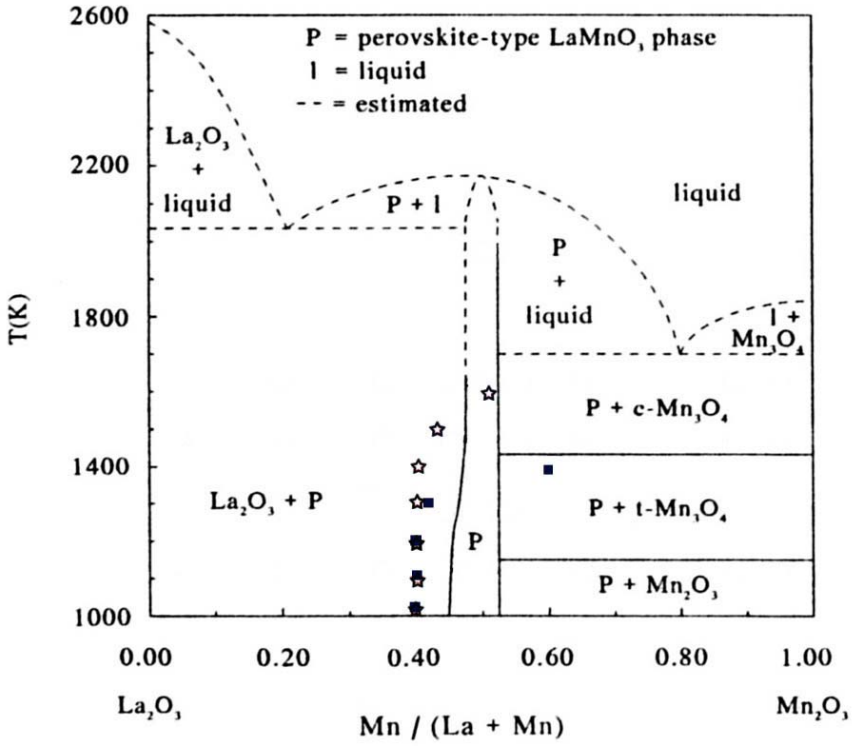

Fig. 16 – Phase diagram of the pseudobinary system La_2O_3-Mn_2O_3 (adapted from [25]), our calculations are represented for the system LMO-2 by squares and for the system LMO-3 - by stars.

1.2. Calculations for the LSM, ULSM systems

The initial conditions for the LSM system correspond to the stoichiometric $La_{1-x}Sr_xMnO_3$ formation, while for the ULSM system they correspond to the substoichiometric $La_{0.65}Sr_{0.3}MnO_3$ formation.

In[24] it is shown that when the plasma gas is a mixture of Ar+H_2 (case LSM-1), the synthesis of Sr doped perovskite is impossible, since in the equilibrium mixture MnO is the only Mn compound in the whole considered temperature range.

When a mixture of Ar+O_2 is used as a plasma gas (cases LSM-2, LSM-3, ULSM), the calculations show that the solid oxides (La_2O_3, Mn_3O_4 and SrO) are contained in the equilibrium mixtures in the temperature range 1400 – 800 K (as examples see Figs. 17, 18). Since these three oxides are responsible for Sr-doped La manganite formation, we can expect its formation in the mentioned temperature range. The doped manganite formation can be determined by the ratio Mn/(La+Mn), (we keep in mind that here, to the difference of the case LMO, the perovskite has a La sub-stoichiometric structure *i.e.* some of the La atoms are replaced by Sr ones). In Fig. 19 the calculated Mn/(La+Mn) ratios for the different considered systems are shown.

We investigate also the ratio La/(La+Sr), comparing it with the ratio values, given in[27] (see Fig. 20). It is shown[27] that the ratio La/(La+Sr) is responsible for the crystal lattice of the obtained perovskite. The comparison between our results and those from[27] leads to the following conclusions: i) for the system LSM-2 the perovskite structure will be stable in the temperature range 1400-800 K and will have rhomdohedral symmetry; ii) for the system LSM-3 the perovskite will be stable in the range 1400–800 K. The cubic symmetry can be expected at the highest temperature (1400 K); after that the rhombohedral one will be typical; iii) for the system ULSM the produced perovskite will be stable in the temperature range 1300–800 K and cubic crystal lattice can be expected.

A comparison between these theoretical predictions about the perovskite crystal structures and XRD investigations of the samples is made in[24] and good agreement is found. We investigate also the La_2O_3 contamination of the perovskite, because it is known[21] that the contamination results in a mechanical damage of the perovskite coatings, due to the hygroscopic behavior of La_2O_3.

The performed calculations show that the use of the precursor with low La concentration leads to a production of low contaminated perovskite.

Fig. 17 – Chemical equilibrium contents calculated for the case LSM-2.

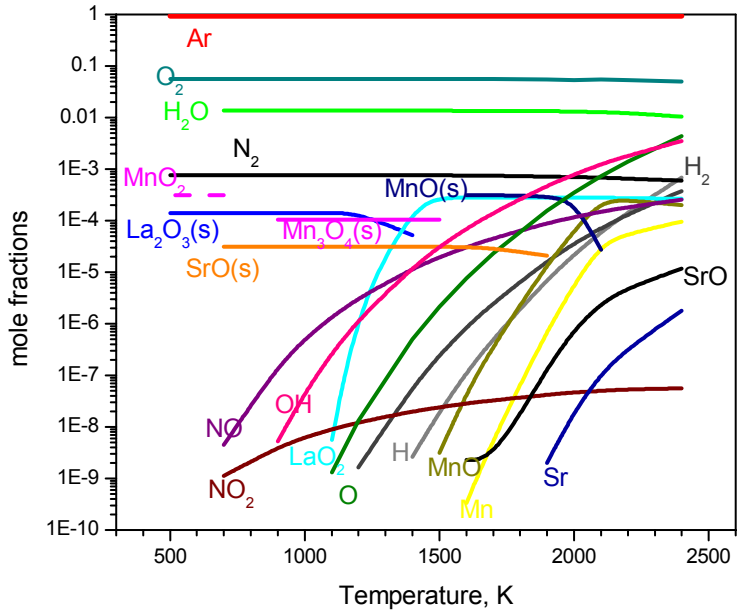

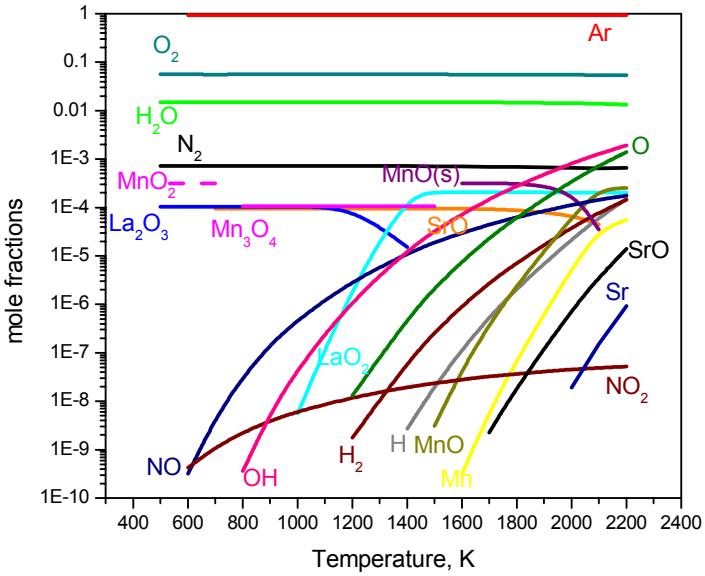

Fig. 18 – Chemical equilibrium contents calculated for the case ULSM.

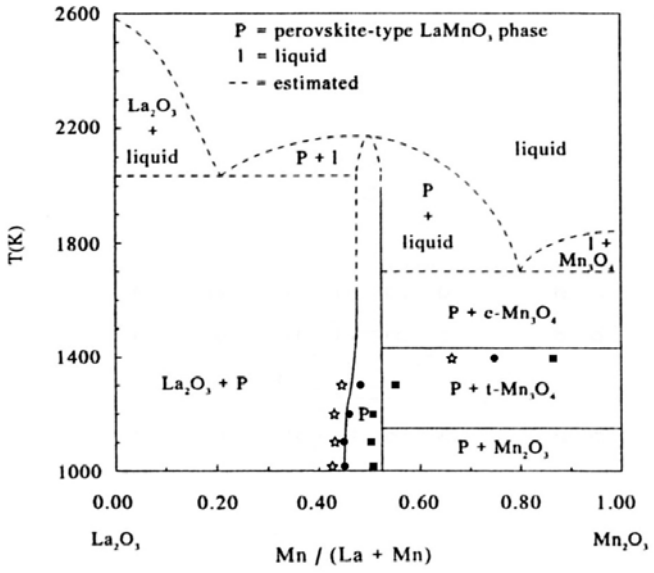

Fig. 19 – Phase diagram of the pseudobinary system La_2O_3-Mn_2O_3 (adapted from [25]), our calculations are represented by: for the system LSM-2- stars; for system LSM-3- circles; for system ULSM -squares.

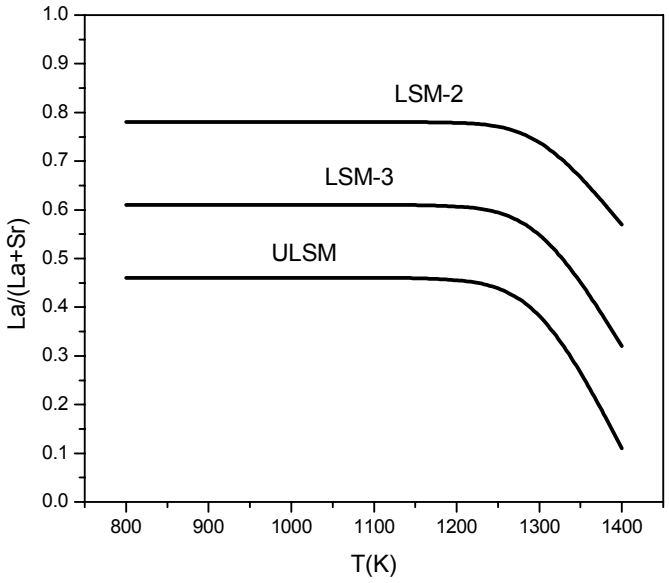

Fig. 20 – Temperature variation of the ratio La/(La+Sr) for systems LSM-2, LSM-3, ULSM. For La/(La+Sr) between 0.5-0.6 the P lattice symmetry becomes rhombohedral, for smaller ratio it is cubic [27].

2. Conclusions from the modelling of the processes of La, (La, Sr) manganite production

These thermodynamic investigations allow to conclude that: in all the considered systems the perovskite structures can be obtained if the plasma gas is $Ar+O_2$ *i.e.* in the oxidizing atmosphere; stable and low contaminated Sr doped perovskites are synthesized predominantly in the temperature range 1200 – 800 K; the predictions about the perovskite crystal structures were confirmed by experimental data of TPCVD perovskite coatings (this is important for planning further experiments).

REFERENCES

1. T. Kodas and M. Hampden–Smith, "Aerosol processing of Materials", New York – Wiley- VCH, 1999.
2. See for example: http://www.space.or, jp; http://www.fuelcelltoday.com.
3. E. G. Balabanova in "Silica 1998" ,Mulhouse, France,1998, p. 67-70.
4. E. Balabanova, A. Levitsky and D. Oliver, *Czech. J. Phys*., **1994,** *44,* 139-152.
5. E. G. Balabanova, and D.H. Oliver, *High Temp.-High Press,* **1997**, *29*, 711-716.
6. E. G. Balabanova, *High Temp.-High Press*., **1998** *30,* 493-500.
7. E. G. Balabanova, "Nanoscience&Nanotechnology- Nanostructured materials application and innovation transfer", E. Balabanova and I. Dragieva (Eds.), Heron press, Sofia, 2001, p. 21-23.
8. E. G. Balabanova, *Vacuum,* **2003,** *69,* 207-212.
9. E. Balabanova, *J. Optoelectronics and Advanced Materials*, **2003**, *5*, 679-686.
10. L.S. Polak (editor) "Plasma chemical reactions and processes" (in Russian), Moscow, "Nauka", 1977, p.164-192.
11. J.Rosinsky and R. Snow, *J. Meteorology*, **1961,** *18*, 1736-1740.
12. E. Pfender, H.Zhu and Y.C. Lau, *Mater. Sci. Eng*. **1991**, *A 139*, 352.
13. E. Bouyer, M. Müller, R. H. Henne and G. Schiller *J. Nanoparticle Research,* **2001,** *3*, 373.
14. E. Bouyer, G. Schiller, M. Müller and R. H. Henne, *Plasma Chem. Plasma Processing*, **2001**, *21*, 523.
15. E. Balabanova, E. Bouyer and M. Müller, "Nanoscience&Nanotehnology -Nanostructured materials application and innovation transfer", E. Balabanova and I. Dragieva (Eds.), Heron Press Science Series 2004, issue 4, p. 22-26.
16. G. B. Sinyarev (editor), "Metod, universalnii algoritm i programma termodinamicheskogo rascheta mnogokomponentnih geterogennih sistem", (Trudi MVTU No 268, 1978) (in Russian).
17. J.A.M. van Roosmalen, *J. Solid State Chemistry*, **1991**, *93*, 212-219.
18. D. Louca, E.I. Brosha and T.Egami, *Phys. Rev*., **2000**, *B 61*, 1351–1356.
19. G. Dezanneau, A. Sin, H. Roussel, M. Audier and H. Vincent, *J. Solid State Chemistry*, **2003,** *1,* 216-226
20. S. F. Miralai, D. Morvan, J. Amouroux, A. Naoumidis, H. Nickel and R. Avni, *Proc. of 12th Int. Symp. on Plasma Chem.*, J. Heberlein (Ed.), Univ. of Minnesota, **1995**, 1999-2004, v.4.
21. H. C. Chen, J. Heberlein and R. Henne, *J. Thermal Plasma Spray Technol*., **2000**, *9,* 348-353.
22. M. Müller, E. Bouyer, M. V .Bradke, D. W. Branston, R. B. Heimann, R. Henne, G. Lins and G. Schiller, *Mat.-wiss. u. Werkstofftechnik,* **2002,** *33*, 322-330.
23. E. Balabanova, and M. Muller, "Nanoscience & Nanotechnology, 5 - Nanostructured materials application and innovation transfer", E. Balabanova and I. Dragieva(Eds.), Heron Press, Sofia, 2005, p. 31-33.
24. E. Balabanova, M. Müller and R. Ruckdaeschel, "Nanoscience & Nanotechnology, 6 Nanostructured materials application and innovation transfer", E. Balabanova and I. Dragieva(Eds.), Heron Press, Sofia, 2006 (in press).
25. J. A. M. van Roosmalen, P. van Vlaaderen and E. H. P. Cordfunke, *J. Solid State Chemistry*, **1995**, *114*, 516-523.
26. P. Majewski, D. Benne, L. Epple and F. Aldinger, *Intern. J. Inorganic Materials,* **2001,** 1257-1259.
27. M. G. Harwood, *The Proc. of the Phys. Soc*., **1995**, *B 68*, 586-592.